

Supporting information for

**A Well-Designed Polymer as a Three-in-One
Multifunctional Binder for High-Performance Lithium-
Sulfur battery**

Jia-Jia Yuan^a, Qing-Ran Kong^a, Zheng Huang^a, You-Zhi Song^a, Ming-Yang Li^b, Li-Feng Fang^a,

Bao-Ku Zhu^{a}, Han-Ying Li^a*

^a Key Laboratory of Macromolecular Synthesis and Functionalization (Ministry of Education),

Department of Polymer Science and Engineering, Zhejiang University, Hangzhou 310027, China

^b Department of Materials Science and Engineering, China University of Mining & Technology

(Beijing), Beijing 100083, China

Corresponding Author

* E-mail: zhubk@zju.edu.cn

Experimental

Materials

Lithium hydroxide (LiOH, 99.9%), N-methyl pyrrolidone (NMP, 99.0%), sublimed sulfur (S, 99.95%), and polyvinyl chloride (PVC, $\bar{M}_w = 80,000$) were supplied from Aladdin Chemistry Co. Ltd. (China) and used without purification. Vinyl chloride-acrylic copolymer (VCA, VC:AA = 7.3:2.7 (wt/wt), $\bar{M}_w = 100,000$) was fabricated by the random free-radical copolymerization as our previous work.¹ Its chemical structures and molecular weight distribution were measured by proton nuclear magnetic resonance (¹H NMR) spectroscopy and gel-permeation chromatography (GPC), respectively (Supporting information, Fig. S1). Polypropylene separators (Celgard 2500) were supplied by Celgard Company (USA). Supper carbon (super P), polyvinylidene fluoride (PVDF), aluminum foil (Al), lithium foil (Li), and other battery materials were provided by Shenzhen Ke-Jing Materials Technology Co. Ltd. (China).

Preparation of LVCA binder

The LVCA binder was prepared by immersing VCA powder into an aqueous LiOH solution (0.1 M) with stirring at room temperature. Then, the treated powder was rinsed with deionized water, and dried in the vacuum oven at 50 °C. The degree of lithium salinization was tested by acid-base titration, and 76.25% of carboxyl groups in VCA powers were lithiated successfully.

Preparation of sulfur cathode

0.6 g supper carbon and 2.4 g sublimed sulfur were mixed by ball milling for 4 h at 200 r/min. The mixture was added into a nitrogen-filled digestion tank and heated in

a closed roaster at 155 °C for 10 h, followed by cooling down to room temperature. And the sulfur–carbon (S/C) composite containing 80 wt% of S was gained. The S/C composite, supper P, and LVCA (7:2:1, wt%) were mixed in NMP with a solid concentration of 15 wt%, and stirred overnight to prepare the cathodic slurry. After that, the obtained slurry was spread on Al foil and put into vacuum oven at 50 °C overnight to dry. Finally, the sulfur cathode using LVCA as binders was obtained, and the sulfur loading of LVCA cathode is about 2.3 mg cm⁻². The cathode using PVDF as binders was fabricated similarly by slurry coating a mixture of the S/C composite, supper P, and PVDF (7:2:1, wt%), and the sulfur loading of PVDF cathode is about 2.1 mg cm⁻².

Physical characterization

The chemical components of VCA and LVCA were characterized using Fourier transform infrared (FT-IR) spectroscopy in a wavenumber range of 4000–600 cm⁻¹. The adhesion strength of the binder was evaluated by peeling off pairs of aluminum strips bonded by binders. The binder solutions were spread onto the aluminum strips, and the two coated areas were overlapped and then dried under vacuum at 60 °C overnight. And three samples of each binder were prepared for testing. For each 15 mm × 60 mm sample, the adhesion strength was tested using a Tensile Test Machine (RGWT-3010, Shenzhen, China), and the extension rate was set to 10 mm min⁻¹. Meanwhile, the sample immersed in the electrolyte overnight was also tested. The electrolyte affinity of binders was evaluated by electrolyte contact angle and uptake of the corresponding homogenized film. And the electrolyte uptake was tested through soaking the films into electrolyte for 2 h and calculated with equation (1):

$$\text{electrolyte uptake (wt\%)} = \frac{W_1 - W_0}{W_0} * 100 \quad (1)$$

where W_1 , W_0 represent the weight of the electrolyte-swelled and dry film, respectively. Absorbance capacity of binders to LiPSs was evaluated by the concentration change of LiPSs solution before and after soaking the binder powder. Typically, LiPSs solution (average formula of Li_2S_6) was prepared by reacting S and Li_2S in 1,2-Dimethoxyethane (DME)/1,3-dioxolane (DOL) mixture (1:1 by volume) in an argon (Ar)-filled glovebox with stirring at 70 °C for 48 h. Different binder powders with the same mass were soaked in the prepared LiPSs solution overnight and the absorbance curves of solutions was measured by UV-vis spectrophotometer (UV5000-PC). The absorbance curves of LiPSs solution with different concentration were tested, and a standard curve of LiPSs solution concentration-absorbance was obtained (Fig. S7). The absorptivity of binders to LiPSs was determined by the absorbance value before and after immersion in LiPSs solution. All binders were dried in 50 °C vacuum oven before soaking in LiPSs solution. All the solution is diluted 10 times before testing the UV absorbance.

The morphologies of the sulfur cathodes before and after cycling were observed using a field emission scanning electron microscopy (FE-SEM, Hitachi S4800, Japan). Elemental mapping was performed on energy dispersive X-ray spectroscopy (EDX, equipped with the FE-SEM). The X-ray photoelectron spectroscopy (XPS) tests of the elements in S cathodes were collected with an Escalab 250Xi spectrometer. The cathode samples after cycling for SEM and XPS testing were took out from disassembled cells in the Ar-filled glove box and immediately rinsed with DME to clean the LiTFSI on

the surface. And then the samples were dried in a vacuum oven at 50 °C for 10 h.

DFT Calculations

All calculations were accomplished by using the density functional theory (DFT) at the B3LYP/6-311+G(2d,p) level in the Gaussian 09 package.² The adsorption binding energy between the binder molecule and Li₂S was gained by subtracting the SCF energies of both binder molecule and Li₂S from the energy of the optimized configuration of binder molecule coordinated to Li₂S. The lowest unoccupied molecular orbital (LUMO) and highest occupied molecular orbital (HOMO) of binder molecule was also calculated.

Battery assembly and electrochemical tests

The 2025 coin-type cells were assembled in a glove box filled with Ar. Li foil and Celgard 2500 separator were selected as the anode and the separator, respectively. The composition of liquid electrolyte is 1 M LiTFSI solution in DME/DOL (1:1, vol%) containing 1 vol% LiNO₃ additive. A shrapnel, a stainless-steel sheet, an anode film, and a separator were placed in an anode cover in turn, and then a drop of electrolyte (20 μL) was added on the top of the separator. After that, a cathode film and a cathode cover were placed sequentially. Finally, the stacked layers were pressed to complete the battery assembly.

The cycle voltammetry (CV) test was carried out using an electrochemical workstation system (CHI 660 C, China) from 1.7 to 2.8 V (vs. Li/Li⁺) at different scan rate (0.1, 0.2, 0.3, 0.4, 0.5 mV s⁻¹) with the assembly of S/PP/Li. S cathode was used as working electrode, and metal Li as both the counter and reference electrodes.

Electrochemical impedance spectroscopy (EIS) was measured by the electrochemical workstation over a frequency range from 1 Hz to 100 kHz in an AC mode. The cycle performance of the assembled S/PP/Li cells was investigated by a Neware BTS-5 V/5 mA battery tester in a potential range of 1.7–2.8 V at 1 C (1000 mA g⁻¹). And the rate capability was tested at various charge/discharge current density from 0.1 C/0.1 C (100 mA g⁻¹) to 2 C/2 C (2000 mA g⁻¹).

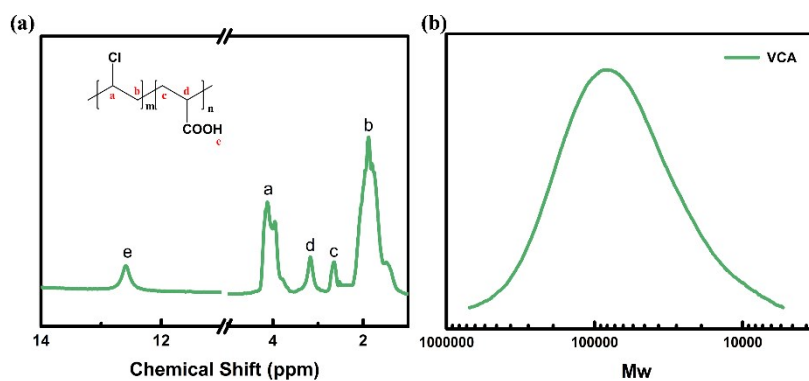


Fig. S1 The chemical structures and molecular weight distribution of VCA polymer.

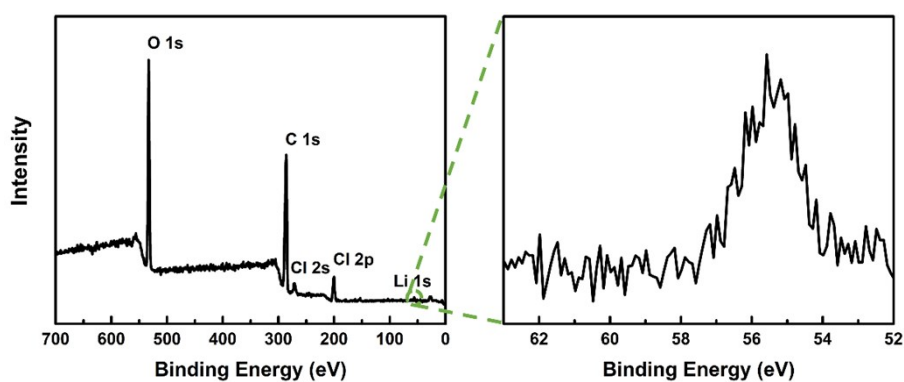


Fig. S2 XPS spectra of LVCA polymer.

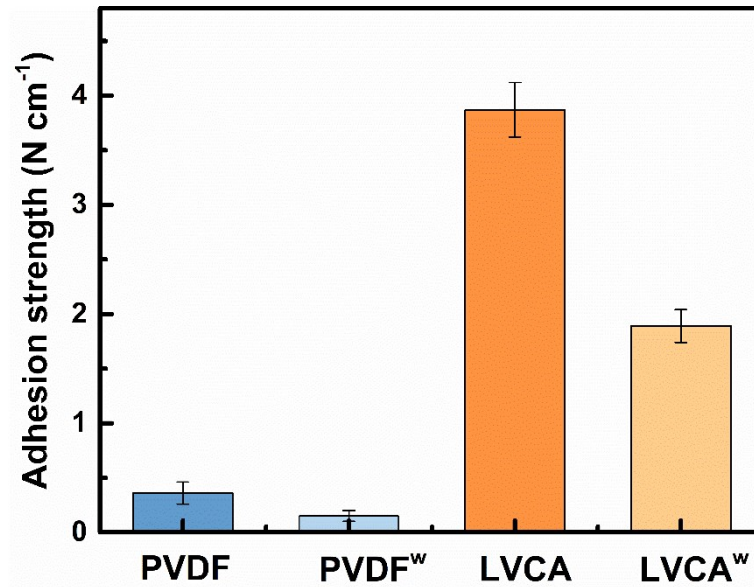


Fig. S3 Adhesion strength between two Al current collectors bonded with different binders measured by the peel test. PVDF, LVCA in the dry state. PVDF^w, LVCA^w in the wet state.

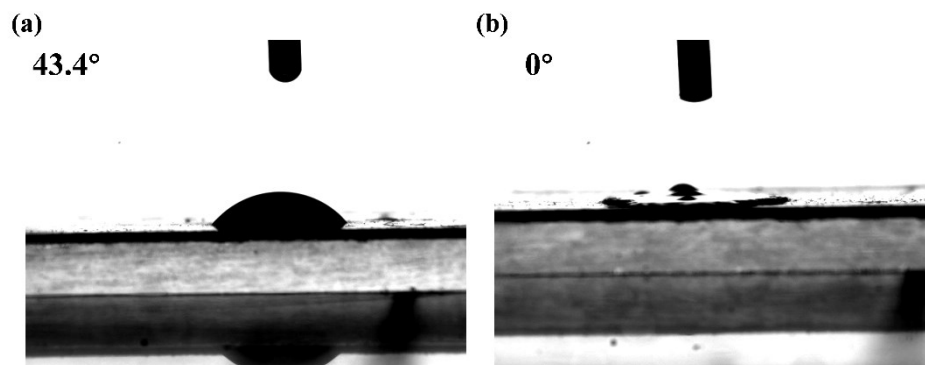


Fig. S4 The contact angle images of LVCA homogeneous film with a) water and b) liquid electrolyte.

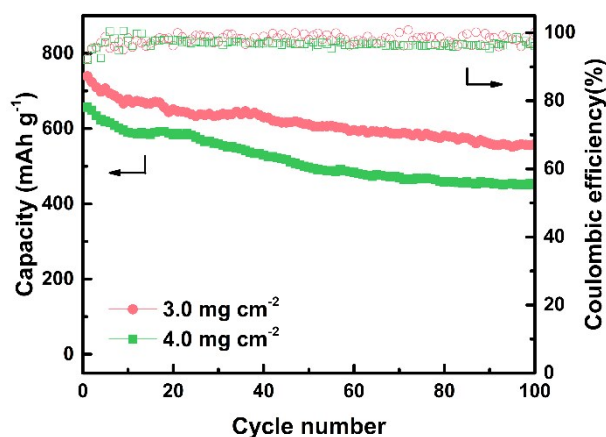


Fig. S5 The charge-discharge profiles and coulombic efficiencies of the LVCA cells with various S loading.

To analyze impedance spectra, fitting results by the equivalent circuit models are shown in Fig. S2a and b. R_e and R_{ct} represent the resistance impedance contributed by the electrolyte and the charge transfer impedance, respectively. W_c is the Warburg impedance caused by the diffusion of lithium polysulfides, CPE is constant phase angle component used to replace capacitance, and R_s is deposit diffusion resistance of the SEI.

Table S1. Fitting results for PVDF and LVCA-based Li-S batteries after cycling.

| Cell | R_e (Ω) | R_{ct} (Ω) | R_s (Ω) |
|-------------------|--------------------|-----------------------|--------------------|
| PVDF ^a | 1.95 | 34.10 | - |
| LVCA ^a | 1.62 | 19.45 | - |
| PVDF ^b | 7.34 | 40.31 | 11.09 |
| LVCA ^b | 2.75 | 13.43 | 9.23 |

^{a)} The cells after 1 cycle; ^{b)} The cells after 800 cycles.

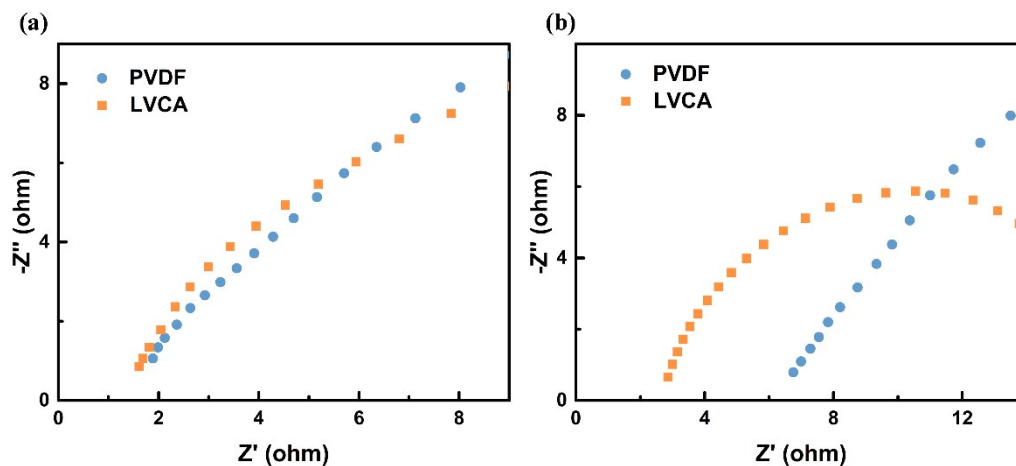


Fig. S6 The high-frequency regions in the EIS plots after a) 1 and b) 800 cycles.

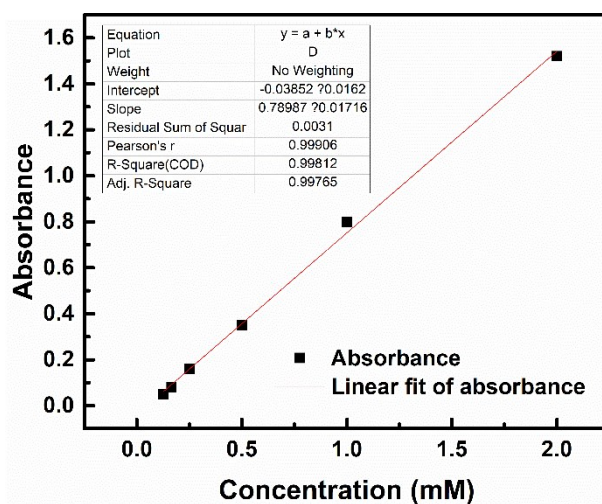


Fig. S7 The LiPSs solution concentration-absorbance curve.

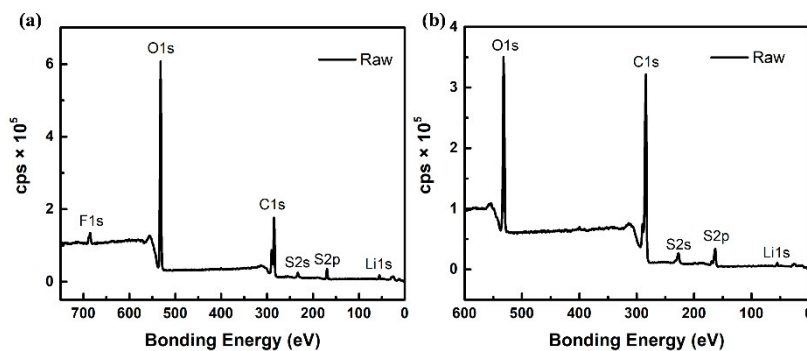


Fig. S8 XPS spectra of the sulfur cathode after discharge: a) wide spectral scan of PVDF cathode,

b) wide spectral scan of LVCA cathode.

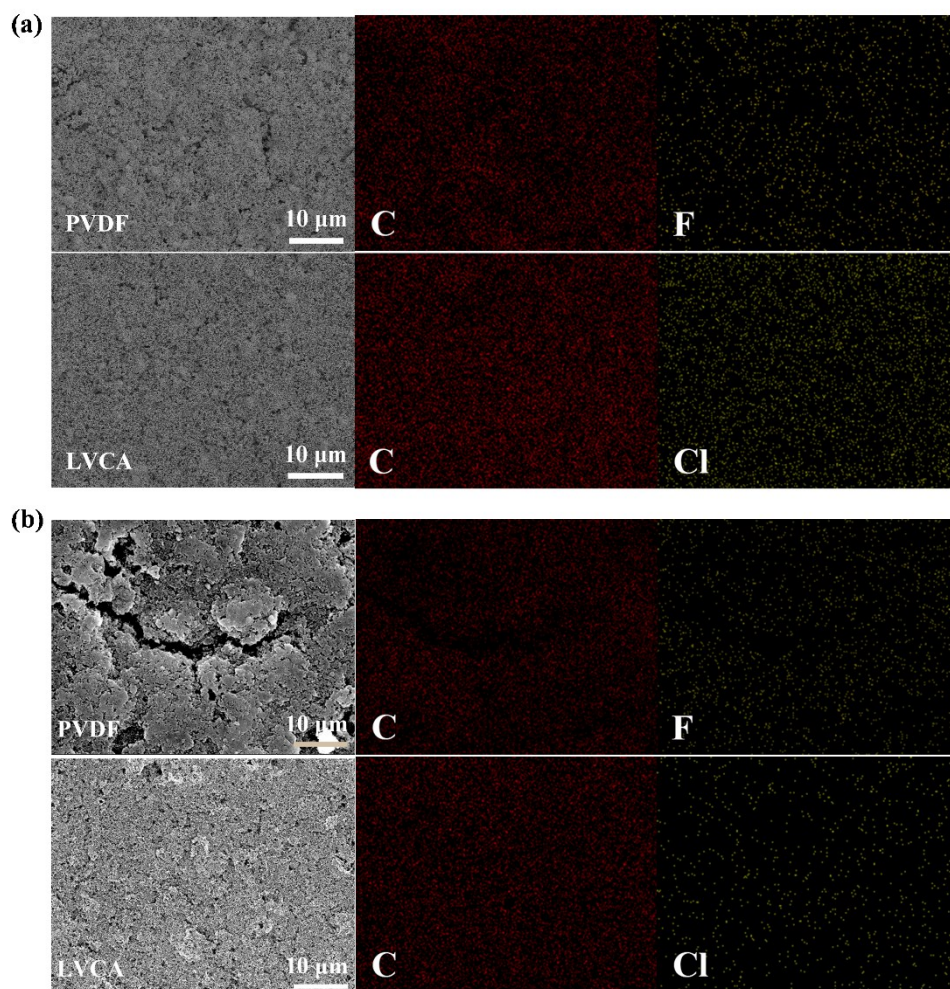


Fig. S9 SEM and the corresponding C, F, Cl element distribution images of the S cathodes with PVDF and LVCA binders (a) before and (b) after cycling (for 800 cycles).

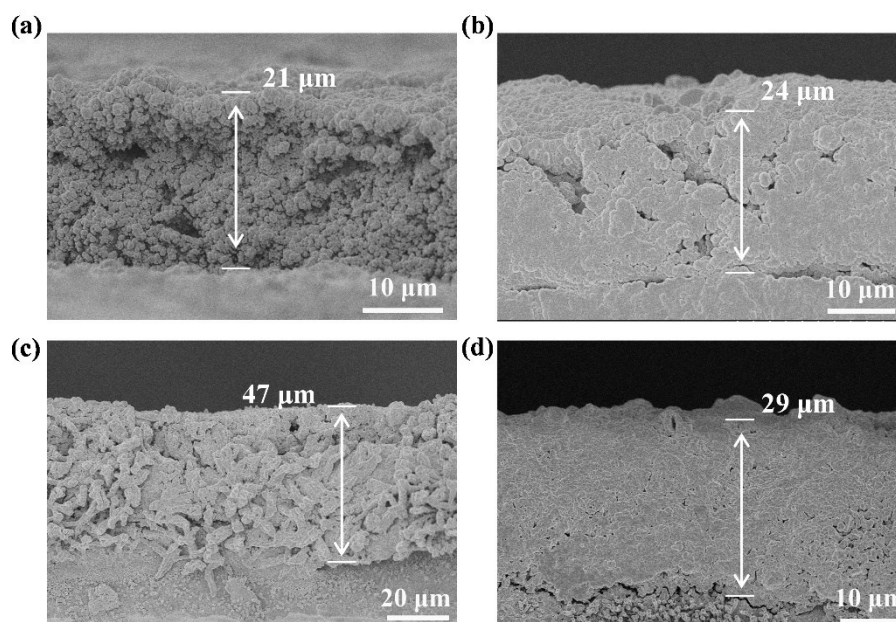


Fig. S10 Cross-section SEM images of the S cathodes with LVCA binders a) before and b) after immersing in the electrolyte (for 24 h); c) the fully-discharged and d) fully-charged state after 10 cycles.

Table S2 Comparison of selected binders for S cathodes.

| Binders | S loading (mg cm ⁻²) | Rate | Cycles | Capacity decay rate per cycle (%) | Ref. |
|------------------|----------------------------------|-------|--------|-----------------------------------|-----------|
| PSF-Im | 1.0–1.1 | 0.2 C | 100 | 0.23 | 3 |
| LiPAACA-Laponite | 1 | 0.5 C | 500 | 0.056 | 4 |
| LBSIP | - | 0.5 C | 500 | 0.06 | 5 |
| CCS | 1.3-1.5 | 0.5 C | 400 | 0.05 | 6 |
| Li41 | 3.0 | 0.5 C | 400 | 0.10 | 7 |
| GPC | 1.4 | 0.5 C | 100 | 0.12 | 8 |
| GOPAA | 0.8 | 0.5 C | 100 | 0.22 | 9 |
| PAA | 0.8 | 0.5 C | 100 | 0.26 | 9 |
| PEB | 1.0 | 0.2 C | 100 | 0.28 | 10 |
| PAMAM | 4.0 | 0.2 C | 100 | 0.15 | 11 |
| PI/PEO | 0.8-1.0 | 0.2 C | 50 | 0.44 | 12 |
| AFG | 3.0 | 0.5 C | 200 | 0.07 | 13 |
| GA | 0.7 | 0.2 C | 500 | 0.05 | 14 |
| PVP | 0.5-0.8 | 1.0 C | 200 | 0.17 | 15 |
| PVP/PEO | 0.5-0.8 | 1.0 C | 200 | 0.15 | 15 |
| C-β-CD | 3.0 | 0.2 C | 50 | 0.11 | 16 |
| PTFE | 3.0 | 0.2 C | 50 | 0.67 | 16 |
| LVCA | 2.3 | 1.0 C | 800 | 0.04 | This work |

PSF-Im: imidazolium polyarylether sulfone; LiPAACA-Laponite: Laponite ($[Mg_{5.34}Li_{0.66}Si_8O_{20}(OH)_4]Na_{0.66}$) crosslinked poly(acryloyl-6-aminocaproic acid); LBSIP: lithium borate containing single ionconducting polymer; CCS: catechol conjugated chitosan sulfate; Li₄1: lithiated redox-mediating supramolecular binder based on perylene bisimide; GPC: a gelatin-polyethylenimine composite; PAA: polyacrylic acid; GOPAA: graphene oxide/PAA; PEB: polyelectrolyte binder; PAMAM: polyamidoamine; PI: polyimide; PEO: poly(ethylene oxide); AFG: the polymerization of hexamethylene diisocyanate (HDI) with PEI; GA: gum Arabic; PVP:

polyvinyl pyrrolidone; C- β -CD: carbonyl- β -cyclodextrin; PTFE: polytetrafluoroethylene.

Reference:

- 1 N. Wang, J. Wang, P. Zhang, W. Wang, C. Sun, L. Xiao, C. Chen, B. Zhao, Q. Kong and B. Zhu, *Front. Chem. Sci. Eng.*, 2018, **12**, 262–272.
- 2 R. Liu, F. Guo, X. Zhang, J. Yang, M. Li, W. Miaomiao, H. Liu, M. Feng and L. Zhang, *ACS Appl. Energy Mater.*, 2019, **2**, 1348–1356.
- 3 F. Wang, L. Li, D. Lei, Y. Li, H. Yang, W. Zhu and F. Zhang, *J. Energy Chem.*, 2020, **43**, 165–172.
- 4 R. Guo, J. Wang, S. Zhang and W.-Q. Han, *Chem. Eng. J.*, 2020, **388**, 124316.
- 5 L. Zhong, Y. Mo, K. Deng, S. Wang, D. Han, S. Ren, M. Xiao and Y. Meng, *ACS Appl. Mater. Interfaces*, 2019, **11**, 28968–28977.
- 6 H. Yi, T. Lan, Y. Yu, Z. Lei, H. Zeng, T. Tang, C. Wang and Y. Deng, *J. Mater. Chem. A*, 2018, **6**, 18660–18668.
- 7 Y. Hwa, P. D. Frischmann, B. A. Helms and E. J. Cairns, *Chem. Mat.*, 2018, **30**, 685–691.
- 8 N. Akhtar, H. Shao, F. Ai, Y. Guan, Q. Peng, H. Zhang, W. Wang, A. Wang, B. Jiang and Y. Huang, *Electrochim. Acta*, 2018, **282**, 758–766.
- 9 G. Xu, Q. Yan, A. Kushima, X. Zhang, J. Pan and J. Li, *Nano Energy*, 2017, **31**, 568–574.
- 10 Z. Yang, R. Li and Z. Deng, *ACS Appl. Mater. Interfaces*, 2018, **10**, 13519–13527.
- 11 M. Ling, L. Zhang, T. Zheng, J. Feng, J. Guo, L. Mai and G. Liu, *Nano Energy*, 2017, **38**, 82–90.
- 12 G. Hernández, N. Lago, D. Shanmukaraj, M. Armand and D. Mecerreyes, *Mater. Today Energy*, 2017, **6**, 264–270.
- 13 W. Chen, T. Qian, J. Xiong, N. Xu, X. Liu, J. Liu, J. Zhou, X. Shen, T. Yang, Y. Chen and C. Yan, *Adv. Mater.*, 2017, **29**, 1605160.
- 14 G. Li, M. Ling, Y. Ye, Z. Li, J. Guo, Y. Yao, J. Zhu, Z. Lin and S. Zhang, *Adv. Energy Mater.*, 2015, **5**, 1500878.
- 15 M. J. Lacey, F. Jeschull, K. Edström and D. Brandell, *J. Power Sources*, 2014, **264**, 8–14.
- 16 J. Wang, Z. Yao, C. W. Monroe, J. Yang and Y. Nuli, *Adv. Funct. Mater.*, 2013, **23**, 1194–1201.